Bio-Inspired Metaheuristics Applied to the Parametrization of PI, PSS, and UPFC–POD Controllers for Small-Signal Stability Improvement in Power Systems

Elenilson V. Fortes[1] · **Luís Fabiano Barone Martins**[2] · **Ednei Luiz Miotto**[3] · **Percival Bueno Araujo**[4] · **Leonardo H. Macedo**[4] · **Rubén Romero**[4]

Abstract

The firefly algorithm (FA) and the artificial bee colony (ABC) algorithm are used in this study to perform a coordinated parametrization of the proportional-integral and supplementary damping controllers, i.e., power system stabilizers (PSSs) and the unified power flow controller (UPFC)–power oscillation damping set. The parametrization obtained for the controllers should allow them to damp the low-frequency oscillatory modes in the power system for different loading scenarios. The power system dynamics is represented using a model based on current injections, known as the current sensitivity model, which implies that a formulation by current injections for the UPFC should be formulated. To validate the proposed optimization techniques and the current injection model for the UPFC for small-signal stability, simulations are carried out under two distinct perspectives, namely, static and dynamic analysis, using the New England system. The results demonstrated the effectiveness of the UPFC's current injection model. Moreover, it was possible to verify that the FA performed better than the ABC algorithm to solve the discussed problem, accrediting both the UPFC current injection model and the FA algorithm as new tools for small-signal stability analysis in electrical power systems.

Keywords Artificial bee colony · Current sensitivity model · Firefly algorithm · POD · PSS · UPFC

✉ Elenilson V. Fortes
  elenilson.fortes@ifg.edu.br

  Luís Fabiano Barone Martins
  luis.martins@ifpr.edu.br

  Ednei Luiz Miotto
  edneimiotto@utfpr.edu.br

  Percival Bueno Araujo
  percival@dee.feis.unesp.br

  Leonardo H. Macedo
  leohfmp@ieee.org

  Rubén Romero
  ruben.romero@unesp.br

[1] Goiás Federal Institute of Education, Science, and Technology, Av. Presidente Juscelino Kubitschek 775, Residencial Flamboyant, 75804-714 Jataí, GO, Brazil

[2] Paraná Federal Institute of Education, Science, and Technology, Av. Doutor Tito s/n, Jardim Panorama, Jacarezinho, PR 86400-000, Brazil

[3] Federal Technological University of Paraná, R. Cristo Rei, 19, Vila Becker, Toledo, PR 85902-490, Brazil

[4] São Paulo State University, Avenida Brasil, 56, Centro, Ilha Solteira, SP 15385-000, Brazil

1 Introduction

Electric power networks are increasingly subjected to situations of excessive loading as the demand for electrical energy grows, resulting in unacceptable voltage levels and frequency deviations. These facts, combined with the interconnection of different systems via long transmission lines and the operation of automatic voltage regulators (AVRs) with high gains and low time constants (DeMello & Concordia, 1969), result in the emergence of low-frequency electromechanical oscillations capable of compromising power system stability and operation (Anderson & Fouad, 2003). The local (0.7–2.0 Hz) and interarea (0.1–0.8 Hz) electromechanical oscillatory modes are of higher importance Kundur (1994), and must be adequately damped for power systems to operate safely.

DeMello and Concordia (1969) were pioneers in studies involving synchronizing and damping torques in weakly-damped power systems. In their article, it is possible to verify

that the AVRs of fast actuation (with low time constants and high gains) provide significant improvements to the limits of stability of permanent regime for the systems when they are subjected to disturbances. However, under high loading conditions associated with weak transmission systems, the actuation of AVRs becomes inefficient.

To mitigate the negative impacts of AVR actuation on power system stability, another controller, called power system stabilizer (PSS), is added to the synchronous machines' excitation systems. Its goal is to add electric torque in phase with changes in the rotor's angular speed (damping torque) (DeMello & Concordia, 1969; Larsen & Swann, 1981). When the PSSs' control settings are properly parametrized, they perform well, especially for local modes (Fortes et al., 2018). In some situations, however, the PSSs may not be capable of damping the interarea oscillatory modes (Fortes et al., 2018).

Flexible ac transmission systems (FACTS) appear to be an appealing alternative because, in addition to improving power system operation (Hingorani, 2000), they can damp interarea oscillations when used in conjunction with a power oscillation damping (POD) controller (Fortes et al., 2018; Miotto et al., 2018).

Among the many existing FACTS, the unified power flow controller (UPFC) stands out as one of the most comprehensive, allowing the control (simultaneously or not) of active and reactive power flows in the transmission line in which its series converter is installed, as well as controlling the voltage on the bus to which the shunt converter is connected (Eslami et al., 2014).

For the PSSs and the UPFC–POD controllers to perform satisfactorily, i.e., for them to be able to damp the local and interarea modes, their correct parameterization is essential, guaranteeing the stability of the power system. To achieve this goal, different approaches have been used over decades of research, including the residue method (Yang et al., 1998), the Nyquist stability criterion (Zhenenko & Farah, 1984), and the decentralized modal control (DMC) method (Valle & Araujo, 2015). The parametrization of these devices in a coordinated and simultaneous fashion is a difficult multimodal optimization problem. As a result, in addition to traditional control theory techniques, metaheuristics have been utilized to address optimization problems in recent studies in this field.

In general, in the literature, studies related to small-signal stability analysis in power systems are restricted to the use of PSSs. These are intended to ensure additional damping to the poles of interests present in power systems, as can be seen in Devarapalli and Bhattacharyya (2021); Movahedi et al. (2019); Singh et al. (2019), and Guesmi et al. (2021). It is essential to note, however, that PSSs alone are not always successful in adding extra damping to the poles of interest in

power systems, particularly for interarea modes, as observed in Fortes et al. (2016).

The use of FACTS together with the POD controller has been an alternative to provide extra damping to the interarea modes, as can be seen in the works of Fortes et al. (2018); Gamino and Araujo (2017); Menezes et al. (2016); Valle and Araujo (2015), and Fortes et al. (2016).

The correct parametrization of PSS and/or POD controllers in order to add additional damping to the poles of interest present in power systems is a current challenge and has been the focus of study in several works available in the literature. Among the techniques used for this purpose, it is possible to highlight bio-inspired metaheuristics such as the genetic algorithm (GA) (Movahedi et al., 2019; Singh et al., 2019), particle swarm optimization (PSO) (Verdejo et al., 2020), bacterial foraging optimization (BFO) (Miotto et al., 2018), artificial bee colony (ABC) (Fazeli-Nejad et al., 2019), harmony search (Naderipour et al., 2020), and the firefly algorithm (FA) (Naderipour et al., 2020; Singh et al., 2019).

In Sabo et al. (2020), three optimization algorithms, i.e., GA, PSO, and a new metaheuristic called farmland fertility algorithm (FFA) were implemented and compared. The objective was to adjust the parameters of the PSSs and verify which of the implemented algorithms has the best performance. In Rahman et al. (2021), differential evolution (DE), PSO, gray wolf optimizer (GWO), whale optimization algorithm (WOA), and chaotic whale optimization algorithm (CWOA) were used in a single machine infinite bus system (SMIB) to adjust the parameters of the proportional-integral (PI) controller. Finally, in Kar et al. (2021), the modified sine cosine algorithm (MSCA) was used to adjust the parameters of PSSs in a SMIB system and a multi-machine system.

It should be mentioned that the power system is represented in this study using the current sensitivity model (CSM) (Takahashi et al., 2018). The CSM has a significant advantage over other linear models available in the literature, for example when compared to the (Heffron & Phillips, 1952) model. Indeed, in the CSM there is no need to maintain the infinite bus nor to reduce the power system to the terminal buses of the generators, which is, therefore, a differential of this work compared to the others mentioned above.

Differently from the works mentioned above, this work investigates the performance of the UPFC FACTS for controlling the active and reactive power flows, as well as voltage magnitudes, at its installation terminal buses, in order to improve the voltage profile of the power system for a specified loading range. Additionally, its influence on maintaining the stability of the system for small-signal disturbances when acting together with supplementary controllers, i.e., PSSs and POD, is evaluated. As a result, a linear model, based on current injections for the UPFC, which can be used for both static and dynamic analysis is used (Martins et al., 2017).

The currents are calculated by an expanded formulation of the power flow and differently from the model proposed in Kopcak et al. (2007), the presented proposal uses the residues of the current injection equations expressed in polar coordinates. The UPFC's control system is based on PI controllers, similar to the one shown in Valle and Araujo (2015), with the difference that, in this work, it is connected to the shunt voltage source converter (VSC).

The parametrization of the supplementary damping controllers and the PI controllers of the UPFC is formulated as an optimization problem composed of two objective functions. Differently from what was proposed in Martins et al. (2017), in which a modified ABC algorithm was used to parametrize the supplementary damping controllers, in this work, the parametrization is performed using the ABC algorithm and the FA, and their performances to solve the problem are evaluated and compared. Two objective functions are considered for evaluating a solution proposal. The first one calculates the minimum desired damping for the oscillatory modes analyzed, while the second one evaluates the distance between the desired and the calculated eigenvalues of interest. The optimization of these functions determines the parametrization of the controllers, which will be able to simultaneously allocate all the electromechanical oscillation modes of the power system in a predetermined region of the left half-plane of the complex plane, guaranteeing the stability of the power system. The New England multimachine system (Fortes et al., 2016) considering multiple loading scenarios is used to evaluate the performances of the ABC algorithm and the FA.

The main contributions of this work are:

(i) To deduce and present a current injection model for UPFC to be used in the CSM for small-signal stability studies;
(ii) To implement the deduced model for the UPFC and perform a static analysis of its operation in order to validate the proposed model;
(iii) To deduce and implement the dynamic models for PI, PSSs, and the UPFC–POD controllers in the CSM for multi-machine systems;
(iv) To present and implement the ABC algorithm and the FA, so that these algorithms can perform, in a coordinated and simultaneous way, the adjustments of the parameters of the PI, PSSs, and the UPFC–POD controllers;
(v) To validate the ABC algorithm and FA as tools in the study of small-signal stability in power systems.

The remainder of this work is organized as follows: Sect. 2 describes the modeling of the electric power system, Sect. 3 presents the parametrization techniques for supplementary damping controllers, in Sect. 4 the problem formulation is described, with emphasis on the objective function used to evaluate a solution proposal. Section 5 presents the simula-
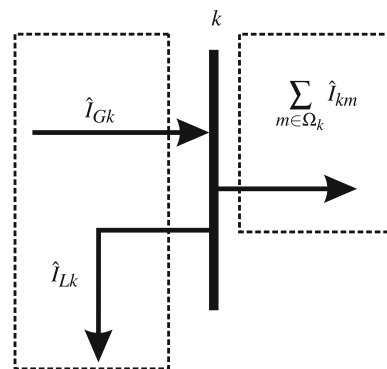

Fig. 1 Balance of the current at bus k

tions and results and Sect. 6 presents the conclusions of the work.

2 The Electric Power System Modeling

Subsections 2.1–2.5 present the main equations that represent the expanded power flow modeled by current injections in the polar form. Besides that, the current injection model for the UPFC FACTS and its control structure, based on PI controllers, are also presented.

2.1 Expanded Current Injection Model

The residue of the currents injected at bus k, $\Delta \hat{I}_k$, is determined from the balance between the specified, $\hat{I}_k^{\text{spe}}$, and calculated, $\hat{I}_k^{\text{calc}}$, current phasors, according to (1) and as illustrated in Fig. 1.

$$\Delta \hat{I}_k = \hat{I}_k^{\text{spe}} - \hat{I}_k^{\text{calc}} = \hat{I}_{Gk} - \hat{I}_{Lk} - \sum_{m \in \Omega_k} \hat{I}_{km} = 0 \qquad (1)$$

The variables $\hat{I}_{Gk}$, $\hat{I}_{Lk}$, and $\hat{I}_{km}$, shown in (1), represent, respectively, the phasors of the currents generated and consumed at bus k and the current between buses k and m. The set of all neighboring buses of bus k is denoted by Ω_k.

Equation (1) can be reformulated according to the active and reactive powers specified in the conventional power flow equations, P_k^{spe} and Q_k^{spe}, together with the voltage phasor at bus k, $\hat{V}_k$, resulting in (2).

$$\Delta \hat{I}_k = \frac{P_k^{\text{spe}} - j Q_k^{\text{spe}}}{\hat{V}_k} - \sum_{m \in \Omega_k} \hat{I}_{km} = 0 \qquad (2)$$

Equations (3) and (4) define, respectively, the magnitude and angle of the voltage at bus k, V_k and θ_k, and the current

phasor $\hat{I}_{km}$.

$$\hat{V}_k = V_k \left(\cos \theta_k + j \sin \theta_k \right) \tag{3}$$

$$\sum_{m \in \Omega_k} \hat{I}_{km} = \sum_{m \in K} V_m \left(G_{km} + j B_{km} \right) \left(\cos \theta_m + j \sin \theta_m \right)$$

$$= \hat{I}_k^{\text{calc}} \tag{4}$$

In (4), the conductance and the susceptance between buses k and m are, respectively, G_{km} and B_{km}. The set Ω_k represents all the buses m connected to bus k, while K represents the set formed from the union of the set Ω_k and the bus k itself.

Replacing (3) and (4) in (2) and separating into real, ΔI_{rk}, and imaginary, ΔI_{ik}, parts, the components of the current residues are obtained for bus k, as shown in (5) and (6).

$$\Delta I_{rk} = \frac{1}{V_k} \left(P_k^{\text{spe}} \cos \theta_k + Q_k^{\text{spe}} \sin \theta_k \right)$$

$$- \sum_{m \in K} V_m \left(G_{km} \cos \theta_m - B_{km} \sin \theta_m \right) = 0 \tag{5}$$

$$\Delta I_{ik} = \frac{1}{V_k} \left(P_k^{\text{spe}} \sin \theta_k - Q_k^{\text{spe}} \cos \theta_k \right)$$

$$- \sum_{m \in K} V_m \left(G_{km} \sin \theta_m + B_{km} \sin \theta_k \right) = 0 \tag{6}$$

The matrix formulation (7) is derived by using the Newton-Raphson method in (5) and (6). It is a linearized system that is utilized to calculate the algebraic variables.

$$\underbrace{\begin{bmatrix} \Delta \mathbf{I}_r \\ \Delta \mathbf{I}_i \end{bmatrix}}_{\Delta \mathbf{I}} = \begin{bmatrix} \overbrace{\frac{\partial \Delta \mathbf{I}_r}{\partial \boldsymbol{\theta}}}^{\mathbf{J4}_{\text{pf}}^{11}} & \overbrace{\frac{\partial \Delta \mathbf{I}_r}{\partial \mathbf{V}}}^{\mathbf{J4}_{\text{pf}}^{12}} \\ \hline \underbrace{\frac{\partial \Delta \mathbf{I}_i}{\partial \boldsymbol{\theta}}}_{\mathbf{J4}_{\text{pf}}^{21}} & \underbrace{\frac{\partial \Delta \mathbf{I}_i}{\partial \mathbf{V}}}_{\mathbf{J4}_{\text{pf}}^{22}} \end{bmatrix} \underbrace{\begin{bmatrix} \Delta \boldsymbol{\theta} \\ \Delta \mathbf{V} \end{bmatrix}}_{\Delta \mathbf{y}} \tag{7}$$

2.2 Current Residue Equations

The residues of the active, ΔP_k, and reactive, ΔQ_k, powers injected at bus k can be expressed as a function of the residues of the real and imaginary components, ΔI_{rk} and ΔI_{ik}, of the current injection at bus k, as shown in (8) and (9).

$$\Delta P_k = \Delta P_k^{\text{spe}} - \Delta P_k^{\text{calc}} = V_k \left(\Delta I_{rk} \cos \theta_k + \Delta I_{ik} \sin \theta_k \right) \tag{8}$$

$$\Delta Q_k = \Delta Q_k^{\text{spe}} - \Delta Q_k^{\text{calc}} = V_k \left(\Delta I_{rk} \sin \theta_k - \Delta I_{ik} \cos \theta_k \right) \tag{9}$$
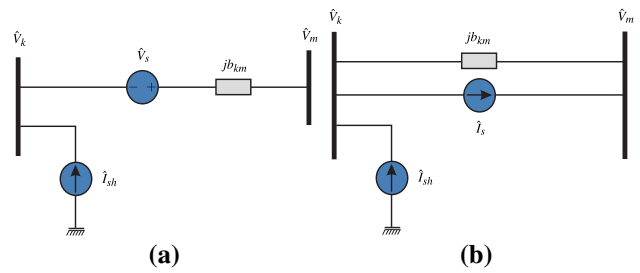

Fig. 2 **a** UPFC's model; **b** representation of the series voltage source as a current source

In (8) and (9), P_k^{calc} and Q_k^{calc} are the active and reactive power injections calculated at bus k. In addition, the manipulation of (8) and (9) allows to determine (10) and (11). These equations represent the components of the current residues as a function of the active and reactive power residues, which are used in the conventional formulation of the power flow problem.

$$\Delta I_{rk} = \frac{\Delta P_k \cos \theta_k + \Delta Q_k \sin \theta_k}{V_k} = 0 \tag{10}$$

$$\Delta I_{ik} = \frac{\Delta P_k \sin \theta_k - \Delta Q_k \cos \theta_k}{V_k} = 0 \tag{11}$$
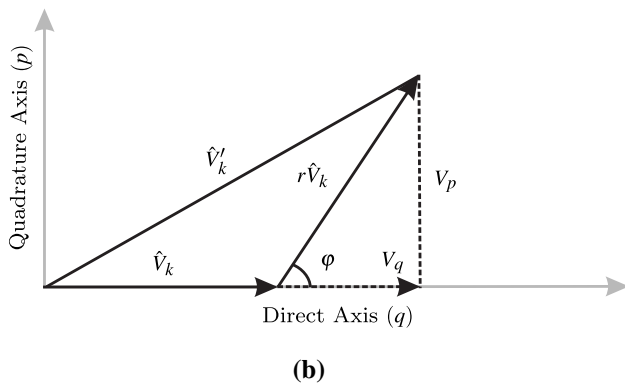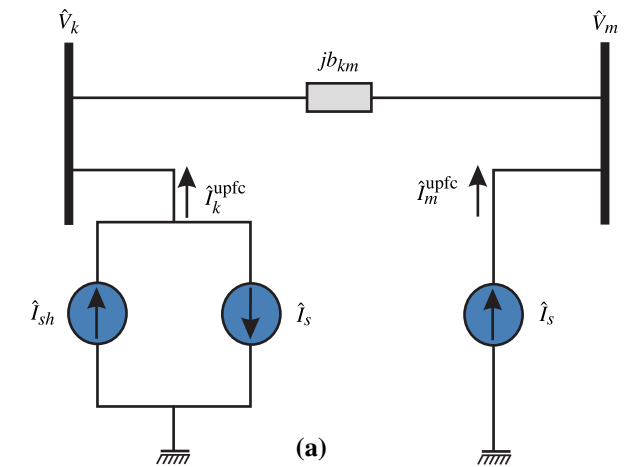
2.3 The UPFC's Current Injection Model

The UPFC is a FACTS that consists of two voltage source converters (VSCs), one shunt and one in series with the transmission line, which are connected to the power system via coupling transformers and generate three-phase sinusoidal voltages at the network frequency with controllable amplitude and phase angle (Hingorani, 2000). The converters are connected by a direct current link and it has a capacitor bank capable of supplying reactive power to the power system or controlling the voltage of the device's common installation bus.

The UPFC's current injection model is achieved by modifying the power injection model proposed by Noroozian et al. (1997), as shown in Fig. 2a. In this model, the equivalent circuit of the UPFC connected to the power system is represented by an ideal voltage source, $\hat{V}_s$, connected between buses k and m, in series with a susceptance, b_{km}, that models the coupling transformer, and a shunt ideal current source, $\hat{I}_{sh}$.

To calculate the current injections at each bus, the series voltage source, shown in Fig. 2a and in (12), is converted into a current source, $\hat{I}_s$, as illustrated in Fig. 2b and in (13).

$$\hat{V}_s = r V_k \left(\theta_k + \varphi \right) \tag{12}$$

$$\hat{I}_s = -r V_k b_{km} \left[\left(\cos \varphi \sin \theta_k + \sin \varphi \cos \theta_k \right) \right.$$

$$\left. + j \left(\sin \varphi \sin \theta_k - \cos \varphi \cos \theta_k \right) \right] \tag{13}$$

Fig. 3 **a** Transformation of the series current source; **b** phasor diagram of the UPFC

Fig. 4 The UPFC's current injection model

Fig. 5 Control system structure of the UPFC

The current source $\hat{I}_s$ can be represented by using two shunt current sources, as shown in Fig. 3a, in which $\hat{I}_k^{\mathrm{upfc}}$ is the current injected by the UPFC into bus k, while $\hat{I}_m^{\mathrm{upfc}}$ is the current injected into bus m. Figure 3b presents a phasor diagram (Huang et al., 2000), in which the voltage $\hat{V}_s$ is decomposed into two components, one in phase (V_q) and another in quadrature (V_p) with the voltage $\hat{V}_k$, of the common bus of the installation of the device. The parameter $r = \frac{V_p^2 + V_q^2}{V_k}$ and the angular phase is $\varphi = \arctan\left(\frac{V_p}{V_q}\right)$.
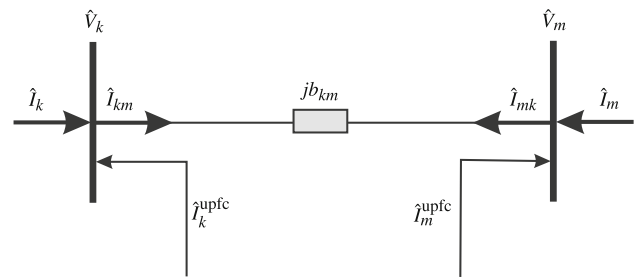
By using (12) and (13) and by analyzing Fig. 3a and b, (14−17) can be obtained.

$$cI_{rk}^{\mathrm{upfc}} = \frac{V_m}{V_k} b_{km} \left(V_p \cos\theta_{km} + V_q \sin\theta_{km}\right)\cos\theta_k$$
$$+ \left(V_q b_{km} + I_q\right)\sin\theta_k \tag{14}$$

$$I_{ik}^{\mathrm{upfc}} = \frac{V_m}{V_k} b_{km} \left(V_p \cos\theta_{km} + V_q \sin\theta_{km}\right)\sin\theta_k$$
$$- \left(V_q b_{km} + I_q\right)\cos\theta_k \tag{15}$$

$$I_{rm}^{\mathrm{upfc}} = -b_{km}\left(V_p \cos\theta_k + V_q \sin\theta_k\right) \tag{16}$$

$$I_{im}^{\mathrm{upfc}} = -b_{km}\left(V_p \sin\theta_k - V_q \cos\theta_k\right) \tag{17}$$

In (14−17), I_{rk}^{upfc} and I_{ik}^{upfc} are the real and imaginary components of the current injection at bus k, while I_{rm}^{upfc} and I_{im}^{upfc} are the real and imaginary components of the current injection at bus m.

From (14−17) it is possible to obtain a current injection model for the UPFC (see Fig. 4), this representation is appropriate for both small-signal stability studies and for static analysis.

2.4 Configuration of the UPFC's Control System

For the UPFC to perform the control of the power flows, it is necessary to use PI controllers (Fortes et al., 2016) as illustrated in Fig. 5. This control structure is used to modulate the controlled variables of the voltage source converters VS1 and VS2, V_p, V_q, and I_p.

In Fig. 5, the parameters of the controllers are the gains K_1^u, K_2^u, and K_3^u (p.u.), the time constants T_1^u, T_2^u, and T_3^u (s) and the time constants T_m^{pod} and T_m (s), which represent the
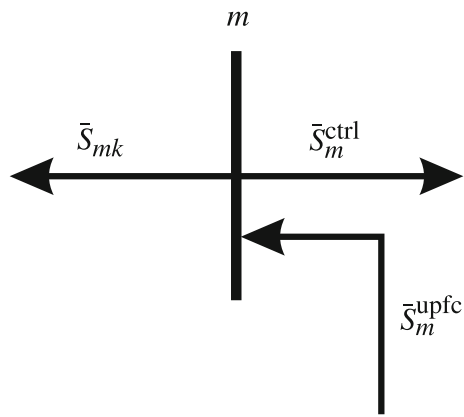
Fig. 6 Power balance at the final bus in which the UPFC is installed

inherent delay of the control device (Hingorani, 2000). The supplementary signal from the POD controller, $V_{\sup}^{\text{pod}}$, is used to modulate the quadrature component, V_p, of the converter VSC1.

The complex power controlled by the UPFC, $\bar{S}_m^{\text{ctrl}} = P_m^{\text{ctrl}} + j Q_m^{\text{ctrl}}$, can be obtained by inspection from Fig. 6, by calculating the nodal power balance at bus m, as shown in (18).

$$\bar{S}_m^{\text{ctrl}} = \bar{S}_m^{\text{upfc}} - \bar{S}_{mk} \tag{18}$$

In (18), $\bar{S}_m^{\text{upfc}}$ and $\bar{S}_{mk}$ represent, respectively, the complex power injected by the UPFC at bus m and the complex power flow from bus m to bus k. The decomposition of the complex power flow (18) in its real and imaginary components makes it possible to determine the active, P_m^{ctrl}, and reactive, Q_m^{ctrl}, power flows controlled by the UPFC.

By analyzing Fig. 5, by inspection, the dynamic performance of the UPFC control structure is obtained, which is represented by (19−24).

$$\dot{V}_p = \frac{K_1^u}{T_m} \left(P_m^{\text{ref}} - P_m^{\text{ctrl}} \right) + \frac{1}{T_m^{\text{pod}}} \left(X_1 - V_p - V_{\sup}^{\text{pod}} \right) \tag{19}$$

$$\dot{X}_1 = \frac{K_1^u}{T_1^u} \left(P_m^{\text{ref}} - P_m^{\text{ctrl}} \right) \tag{20}$$

$$\dot{V}_q = \frac{K_2^u}{T_m} \left(Q_m^{\text{ref}} - Q_m^{\text{ctrl}} \right) + \frac{1}{T_m} \left(X_2 + V_q \right) \tag{21}$$

$$\dot{X}_2 = \frac{K_2^u}{T_2^u} \left(Q_m^{\text{ref}} - Q_m^{\text{ctrl}} \right) \tag{22}$$

$$\dot{I}_q = \frac{K_3^u}{T_m} \left(V_k^{\text{ref}} - V_k \right) + \frac{1}{T_m} \left(X_3 - I_q \right) \tag{23}$$

$$\dot{X}_3 = \frac{K_3^u}{T_3^u} \left(V_k^{\text{ref}} - V_k \right) \tag{24}$$

In (19−24), P_m^{ref}, Q_m^{ref}, and V_k^{ref} are, respectively, the specified values of the active and reactive power flows on line km and the voltage magnitude at bus k.

2.5 Inclusion of the UPFC in the Current Injection Model

In order to assess the UPFC's performance, the respective equations that model the device must be included in the proposed formulation. For this to occur, it must be assumed that the state variables of the model are constant with respect to time, which facilitates their inclusion in the Newton–Raphson algorithm, according to the formulation proposed in Kopcak et al. (2007).

As the purpose of this article is to model the power flow by current injections, the model should satisfy all current residues at the common installation buses of the UPFC, i.e., buses k and m shown in Fig. 4. This requirement is shown in (25) and (26).

$$\hat{I}_k = \hat{I}_k^{\text{spe}} - \hat{I}_k^{\text{calc}} + \hat{I}_k^{\text{upfc}} \tag{25}$$

$$\hat{I}_m = \hat{I}_m^{\text{spe}} - \hat{I}_m^{\text{calc}} + \hat{I}_m^{\text{upfc}} \tag{26}$$

In (25) and (26), $\hat{I}_k^{\text{upfc}}$ and $\hat{I}_m^{\text{upfc}}$ are the phasors representing the current injections at buses k and m, in which the UPFC is installed, whereas, at the other buses of the power system, the residues of the components of the currents do not differ from the conventional power flow formulation.

After linearizing the system formed by the equations resulting from the replacement in (25) of the current injections of the UPFC and of the current residues defined, respectively, in (14–17) and (5–6) and by the set of dynamic equations ($\dot{\mathbf{x}}_u = \mathbf{f}_u(\mathbf{x}_u, \mathbf{y})$) represented in (19–24), the matrix formulation by current injection for the UPFC is obtained, as shown in (27).
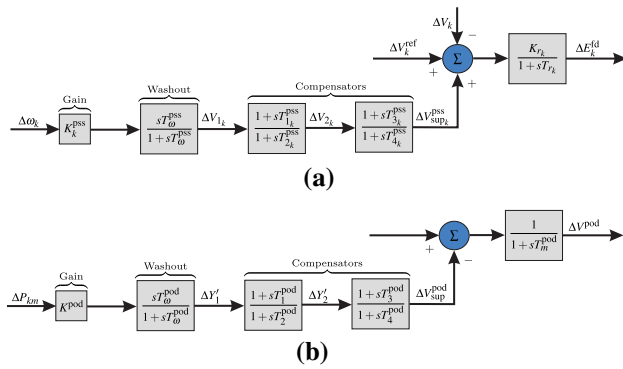

$$\tag{27}$$

Fig. 7 Control structure of **a** the PSSs and **b** the POD controller

In (27), $\Delta \mathbf{x}_u = \begin{bmatrix} \Delta V_p & \Delta X_1 & \Delta V_q & \Delta X_2 & \Delta I_q & \Delta X3 \end{bmatrix}^t$ is the vector of the linearized state variables for the PI controllers of the UPFC, with the matrix $\mathbf{J4}_u$ defined in (28).

$$\mathbf{J4}_u = \begin{bmatrix} 0 \cdots 0 & \cdots & 0 & \cdots & 0 & 0 \cdots 0 & \cdots & 0 & \cdots & 0 \\ & & & & & & & & & \\ 0 \cdots \dfrac{\partial I_{rk}^{\mathrm{upfc}}}{\partial \theta_k} \cdots \dfrac{\partial I_{rk}^{\mathrm{upfc}}}{\partial \theta_m} & \cdots & 0 & 0 \cdots \dfrac{\partial I_{rk}^{\mathrm{upfc}}}{\partial \theta_k} \cdots \dfrac{\partial I_{rk}^{\mathrm{upfc}}}{\partial \theta_m} & \cdots & 0 \\ & & & & & & & & & \\ 0 \cdots \dfrac{\partial I_{rm}^{\mathrm{upfc}}}{\partial \theta_k} \cdots \dfrac{\partial I_{rm}^{\mathrm{upfc}}}{\partial \theta_m} & \cdots & 0 & 0 \cdots \dfrac{\partial I_{rm}^{\mathrm{upfc}}}{\partial \theta_k} \cdots \dfrac{\partial I_{rm}^{\mathrm{upfc}}}{\partial \theta_m} & \cdots & 0 \\ & & & & & & & & & \\ 0 \cdots 0 & \cdots & 0 & \cdots & 0 & 0 \cdots 0 & \cdots & 0 & \cdots & 0 \\ \hline 0 \cdots 0 & \cdots & 0 & \cdots & 0 & 0 \cdots 0 & \cdots & 0 & \cdots & 0 \\ & & & & & & & & & \\ 0 \cdots \dfrac{\partial I_{ik}^{\mathrm{upfc}}}{\partial \theta_k} \cdots \dfrac{\partial I_{ik}^{\mathrm{upfc}}}{\partial \theta_m} & \cdots & 0 & 0 \cdots \dfrac{\partial I_{ik}^{\mathrm{upfc}}}{\partial V_k} \cdots \dfrac{\partial I_{rk}^{\mathrm{upfc}}}{\partial V_m} & \cdots & 0 \\ & & & & & & & & & \\ 0 \cdots \dfrac{\partial I_{im}^{\mathrm{upfc}}}{\partial \theta_k} \cdots \dfrac{\partial I_{im}^{\mathrm{upfc}}}{\partial \theta_m} & \cdots & 0 & 0 \cdots \dfrac{\partial I_{im}^{\mathrm{upfc}}}{\partial V_k} \cdots \dfrac{\partial I_{im}^{\mathrm{upfc}}}{\partial V_m} & \cdots & 0 \\ & & & & & & & & & \\ 0 \cdots 0 & \cdots & 0 & \cdots & 0 & 0 \cdots 0 & \cdots & 0 & \cdots & 0 \end{bmatrix} \tag{28}$$

2.6 Dynamic Models for the PSS and POD Controllers

The supplementary damping controllers used to damp the low-frequency oscillations in the power system are the power system stabilizers (PSSs) and the power oscillation damping (POD). Their structures are presented in Fig. 7a and b, respectively.

As it can be analyzed in Fig. 7a, the PSS is coupled to the AVR, which is represented by a gain K_{r_k}, a time constant T_{r_k}, the terminal voltage ΔV_k, the reference voltage $\Delta V_{\mathrm{ref}_k}$, and the excitation voltage of the synchronous machine ΔE_k^{fd}. In Fig. 7b the POD controller is coupled to the control loop of the UPFC to modulate ΔV^{pod}.

In the structures shown in Fig. 7a and b, there is a great similarity between the PSS and POD controllers, both differ only by the input and output signals used. The controllers have gains K^{pss} and K^{pod}, which are responsible for determining the amount of damping introduced by them; a washout block that functions as a high-pass filter determined by a time constant T_w^{pss} for the PSS and T_w^{pod} for the POD, which is adjusted to allow the controller to act only in transient periods; and a phase compensation block represented by the time constants $T_1^{\mathrm{pss}}(T_1^{\mathrm{pod}})$, $T_2^{\mathrm{pss}}(T_2^{\mathrm{pod}})$, $T_3^{\mathrm{pss}}(T_3^{\mathrm{pod}})$, and $T_4^{\mathrm{pss}}(T_4^{\mathrm{pod}})$ which provides the appropriate phase advance characteristics to compensate the phase delay between the output of the control loop of the AVR and the torque produced by the generator. Usually $T_1^{\mathrm{pss}}(T_1^{\mathrm{pod}}) = T_3^{\mathrm{pss}}(T_3^{\mathrm{pod}})$ and $T_2^{\mathrm{pss}}(T_2^{\mathrm{pod}}) = T_4^{\mathrm{pss}} (T_4^{\mathrm{pod}})$ (Kundur, 1994).

For the input and output signals shown in Fig. 7a and b, the following configurations are adopted: the input signal used for the PSS is the angular speed, $\Delta \omega_k$, of the rotor of the generator k, whereas for the POD it is the active power flow, ΔP_{km}, on the transmission line adjacent to the installation of the UPFC–POD; the output signal for the PSS is the voltage $\Delta V_{\mathrm{sup}}^{\mathrm{pss}}$ added to the control loop of the AVR, as shown in Fig. 7a, while the output signal for the POD is the voltage $V_{\mathrm{pod}}^{\mathrm{sup}}$, added to the control loop of VSC1, as shown in Fig. 5a.

An analysis of Fig. 7a and b allows to infer $(29) - (32)$ and $(33 - 36)$ representing, respectively, the dynamic behaviors of the PSS and POD controllers.

$$\Delta \dot{V}_{1k} = \Delta \dot{\omega}_k K_k^{\mathrm{pss}} - \frac{1}{T_\omega^{\mathrm{pss}}} \Delta V_{1k} \tag{29}$$

$$\Delta \dot{V}_{2k} = \frac{1}{T_2^{\mathrm{pss}}} \Delta V_{1k} + \frac{T_1^{\mathrm{pss}}}{T_2^{\mathrm{pss}}} \Delta \dot{V}_{1k} - \frac{1}{T_2^{\mathrm{pss}}} \Delta V_{2k} \tag{30}$$

$$\Delta \dot{V}_{\mathrm{sup}_k}^{\mathrm{pss}} = \frac{1}{T_4^{\mathrm{pss}}} \Delta V_{2k} + \frac{T_3^{\mathrm{pss}}}{T_4^{\mathrm{pss}}} \Delta \dot{V}_{2k} - \frac{1}{T_4^{\mathrm{pss}}} \Delta V_{\mathrm{sup}_k}^{\mathrm{pss}} \tag{31}$$

$$\Delta \dot{E}_k^{\mathrm{fd}} = \frac{K_{r_k}}{T_{r_k}} \left(\Delta V_{\mathrm{sup}_k}^{\mathrm{pss}} + \Delta V_k^{\mathrm{ref}} - \Delta V_k \right) - \frac{1}{T_{r_k}} \Delta E_k^{\mathrm{fd}} \tag{32}$$

$$\Delta \dot{Y}_1 = -\frac{1}{T_{w_p}} \left(K^{\mathrm{pod}} \Delta P_{km} + \Delta Y_1 \right) \tag{33}$$

$$\Delta \dot{Y}_2 = -\frac{1}{T_2^{\mathrm{pod}}} \left[\left(1 - \frac{T_1^{\mathrm{pod}}}{T_2^{\mathrm{pod}}} \right) \left(K^{\mathrm{pod}} \Delta P_{km} + \Delta Y_1 \right) - \Delta Y_2 \right] \tag{34}$$

$$\Delta \dot{Y}_3 = -\frac{1}{T_4^{\mathrm{pod}}} \left\{ \left(1 - \frac{T_3^{\mathrm{pod}}}{T_4^{\mathrm{pod}}} \right) [\Delta Y_2 \right.$$
$$\left. + \frac{T_1^{\mathrm{pod}}}{T_2^{\mathrm{pod}}} \left(K^{\mathrm{pod}} \Delta P_{km} + \Delta Y_1 \right) \right] - \Delta Y_3 \right\} \tag{35}$$

$$\Delta \dot{V}_p = \frac{1}{T_m^{\mathrm{pod}}} \left\{ K_1^u \left(\Delta P_m^{\mathrm{ref}} - \Delta P_m^{\mathrm{ctrl}} \right) + (\Delta X_1 - \Delta V_p) \right.$$
$$- \left\{ \Delta Y_3 + \frac{T_3^{\mathrm{pod}}}{T_4^{\mathrm{pod}}} [\Delta Y_2 + \right.$$
$$\left. \left. \frac{T_1^{\mathrm{pod}}}{T_2^{\mathrm{pod}}} \left(K^{\mathrm{pod}} \Delta P_{km} + \Delta Y_1 \right) \right] \right\} \right\} \tag{36}$$

2.7 Current Sensitivity Model

A linear model, called CSM, based on Kirchhoff's current law is used to represent the power system (Fortes et al., 2018). An interesting feature of this model is the maintenance of all buses of the system in the model, what makes it possible the integration of FACTS–POD devices and PSS controllers in the network.

The dynamics of a multimachine power system with ng generators, nb buses, np PSSs, and a UPFC–POD set is described by $(37) - (44)$.

$$[\Delta \mathbf{x}_{\text{csm}}] = \left[\left[\Delta\omega_1 \cdots \Delta\omega_{ng}\right] \left[\Delta\delta_1 \cdots \Delta\delta_{ng}\right]\right.$$
$$\left.\left[\Delta E'_{q_1} \cdots \Delta E'_{q_{ng}}\right] \left[\Delta E_{\text{fd}_1} \cdots \Delta E_{\text{fd}_{ng}}\right]\right]^t \quad (37)$$

$$[\Delta \mathbf{x}^{\text{pss}}] = \left[\left[\Delta V_{1_1} \cdots \Delta V_{1_{np}}\right] \left[\Delta V_{2_1} \cdots \Delta V_{2_{np}}\right]\right.$$
$$\left.\left[\Delta V^{\text{pss}}_{\text{sup}_1} \cdots \Delta V^{\text{pss}}_{\text{sup}_{np}}\right]\right]^t \quad (38)$$

$$\left[\Delta \mathbf{x}^{\text{pod}}\right] = \left[\Delta Y_1 \; \Delta Y_2 \; \Delta Y_3 \; \Delta V^{\text{pod}}_{\text{sup}}\right]^t \quad (39)$$

$$[\Delta \mathbf{x}_T] = \left[\Delta x_{g_1} \; \Delta x_1^{\text{pss}} \; \Delta x_u \; \Delta x^{\text{pod}} \cdots \Delta x_{g_{ng}} \; \Delta x_{np}^{\text{pss}}\right]^t \quad (40)$$

$$[\Delta \mathbf{u}_{\text{csm}}] = \left[\left[\Delta P_1^{\text{mec}} \cdots \Delta P_{ng}^{\text{mec}}\right] \left[\Delta V_1^r \cdots \Delta V_{ng}^r\right]\right.$$
$$\left[\Delta P_{L_1} \cdots \Delta P_{L_{ng}}\right]$$
$$\left.\left[\Delta Q_{L_1} \cdots \Delta Q_{L_{ng}}\right]\right]^t \quad (41)$$

$$[\Delta \mathbf{u}_u] = \left[P_m^{\text{ref}} \; P_m^{\text{ref}} \; Q_m^{\text{ref}} \; Q_m^{\text{ref}} \; V_k^{\text{ref}} \; V_k^{\text{ref}}\right]^t \quad (42)$$

$$\left[\Delta \mathbf{y}\right] = [[\Delta\theta_1 \cdots \Delta\theta_{nb}] [\Delta V_1 \cdots \Delta V_{nb}]]^t \quad (43)$$

$$\begin{bmatrix} \Delta\dot{\mathbf{x}}_T \\ 0 \end{bmatrix} = \begin{bmatrix} \mathbf{J1}_T & \mathbf{J2}_T \\ \mathbf{J3}_T & \underbrace{\mathbf{J4}_{\text{pf}} + \mathbf{J4}_u}_{\mathbf{J4}_T} \end{bmatrix} \begin{bmatrix} \Delta\mathbf{x}_T \\ \Delta\mathbf{y} \end{bmatrix} + \begin{bmatrix} \mathbf{B1}_T \\ \mathbf{B2}_u \end{bmatrix} \left[\Delta\mathbf{u}_u\right]$$
$$(44)$$

In (44), the submatrices $\mathbf{J1}_T$, $\mathbf{J2}_T$, $\mathbf{J3}_T$, and $\mathbf{J4}_T$ associate the state variables with the algebraic variables of the system. The state variables are: the angular speed, $\Delta\omega$, the internal angle of the rotor, $\Delta\delta$, the internal quadrature voltage, $\Delta E'_q$, and field voltage of the generators, ΔE_{fd}, the control parameters of the converters VS1 and VS2 of the UPFC, ΔV_p, ΔV_q, and ΔI_p, the auxiliary variables, ΔX_1, ΔX_2, and ΔX_3, the variables of the PSSs, $\Delta V1_k$, $\Delta V2_k$, and ΔV^{pss}, and the variables of the POD controller, $\Delta Y1$, $\Delta Y2$, $\Delta Y3$, and ΔV^{pod}. The algebraic variables are the magnitude, ΔV, and the phase, $\Delta\theta$, of the voltages at the buses of the power system. The input variables are the mechanical power, ΔP^{mec}, the reference voltage of the AVR, ΔV^r, the active, ΔP_L, and reactive, ΔQ_L, loads, the active, ΔP_m^{ref}, and reactive, ΔQ_m^{ref}, power references, and the voltage reference, ΔV_k^{ref}, of the PI controllers of the UPFC, present in the sub-matrices $\mathbf{B1}_T$ and $\mathbf{B2}_u$.

The state space representation is obtained by eliminating $\Delta\mathbf{y}$ from the system defined in (44), which results in the state matrices $\mathbf{A} = \mathbf{J1}_T - \mathbf{J2}_T\mathbf{J4}_T^{-1}\mathbf{J3}_T$ and the input $\mathbf{B} = \mathbf{B1}_T - \mathbf{J2}_T\mathbf{J4}_T^{-1}\mathbf{B2}_u$.

3 Parametrization Techniques for the Supplementary Damping Controllers

The ABC algorithm and the FA, which were used to parametrize the PI and supplementary damping controllers, are described in depth in this section.

3.1 FA

The FA was proposed by Yang in 2007 (Watanabe, 2009; Yang, 2008). The algorithm was conceived from the analysis of the frequency and intensity of the light emitted by these insects.

In the FA, it is assumed that the initial population consists of NP candidate solutions to the optimization problem. Each solution describes the position of a firefly, which is represented by a vector of dimension d containing the variables of the problem. Each solution $\mathbf{z}_i = [z_{i1} \; z_{i2} \; \cdots \; z_{id}]$ has a corresponding objective function value $F(\mathbf{z}_i)$, $i = 1, \cdots, NP$ that corresponds to its quality. The brightness of each firefly is proportional to its corresponding objective function (quality) which, together with their attractiveness factor (β), dictates how strong the attraction of other members of the swarm will be. Also, other constants such as the maximum attraction value (β_0), the absorption coefficient (γ), which determines the variation in attractiveness with increasing distance, and a randomization parameter (α) are also part of the FA and must be defined by the operator.

Two key components of the FA must be specified before it can be implemented: the variation of light intensity and the formulation of the attractiveness factor. In the standard algorithm, the light intensity (I) of a firefly used to represent a solution $\mathbf{z}_i$ is proportional to the value of its objective function. On the other hand, the luminous intensity $I(r_{ij})$ is defined according to (45).

$$I(r) = I_0 \, e^{-\gamma r_{ij}^2} \quad (45)$$

In (45), I_0 is used to indicate the source's light intensity, and the light absorption is estimated using the absorption coefficient γ. The attractiveness factor β of the firefly is proportional to the luminous intensity of its flash, being, therefore, possible to represent it using (46).

$$\beta = \beta_0 \, e^{-\gamma r_{ij}^2} \quad (46)$$

In (46), β_0 is the attractiveness for $r_{ij} = 0$ and γ is the light absorption coefficient of the propagation medium.

In the classical FA, the Euclidean distance r_{ij}, between two fireflies, $\mathbf{z}_i$ and $\mathbf{z}_j$, is expressed as shown in (47).

$$r_{ij} = \|\mathbf{z}_i - \mathbf{z}_j\| = \sqrt{\sum_{k=1}^{d} \left(z_{ik} - z_{jk}\right)^2} \tag{47}$$

In (47), d indicates the dimension of the problem. The movement of the ith firefly is directed to the brightest (most attractive) firefly j as shown in (48).

$$\mathbf{z}_i = \mathbf{z}_i + \beta_0\,e^{-\gamma r_{ij}^2}\left(\mathbf{z}_i - \mathbf{z}_j\right) + \alpha\boldsymbol{\epsilon}_i \tag{48}$$

In (48), $\boldsymbol{\epsilon}_i$ is a vector of random numbers generated using a Gaussian distribution. The firefly's motions are made up of three terms: the current position of the ith firefly, the attraction to the most attractive individual, and a random walk, consisting of a randomization parameter α (random number, considering a uniform distribution, in the interval [0, 1]).

3.2 ABC Algorithm

Artificial bees are divided into three categories by the ABC algorithm: workers, observers, and explorers. Worker bees make up half of the colony, while observation bees make up the other half. Worker bees save knowledge about their food sources' surroundings and transmit it on to observer bees, who prefer to choose the best sources among those supplied by workers. Then they focus their search on the food source they have chosen. The explorer bees are worker bees that quit their food sources at random and seek out new ones. The ABC algorithm's stages are outlined below.

3.2.1 Population Initialization

The initial population of potential solutions consists of SN food source locations. An initial food source, $\mathbf{z}_i = [z_{i1}\ z_{i2} \cdots z_{id}]$, is a randomly generated d-dimensional vector that represents the optimization parameters, as shown in (49).

$$z_{ij} = z_{ij}^{\min} + \epsilon_{ij}\left(z_{ij}^{\max} - z_{ij}^{\min}\right) \tag{49}$$

In (49) $i = \{1, 2, \cdots, SN\}$ and $j = \{1, 2, \cdots, d\}$. On the other hand, $z_{ij}^{\min}$ and $z_{ij}^{\max}$ are, respectively, the lower and upper bounds of each optimization parameter and ϵ_{ij} is a random number generated in the range [0, 1]. Each of the SN food sources will be occupied by a worker bee and the value of $F(\mathbf{z}_i)$ (objective function) must be evaluated.

3.2.2 Bee Phase Initialization

Using the search equation (50), each worker bee positioned at $\mathbf{z}_i$ produces a new food source $\mathbf{v}_i$ in the neighborhood of its present position.

$$v_{ij} = z_{ij} + \Phi\left(z_{ij} - z_{kj}\right) \tag{50}$$

In (50), $k \in \{1, 2 \cdots, SN\}$ and $j \in \{1, 2, \cdots, d\}$ are indices randomly chosen, with k different from i, while Φ_{ij} is a random number between $[-1, 1]$.

After determining $\mathbf{v}_i$, it will be evaluated and compared to $\mathbf{z}_i$. A greedy selection process is employed between old and new candidate solutions. If the objective function of $\mathbf{v}_i$ is better than or equal to the objective function of $\mathbf{z}_i$, then $\mathbf{v}_i$ will replace $\mathbf{z}_i$ in the population. Otherwise, $\mathbf{z}_i$ will be maintained.

3.2.3 Probabilistic Selection

After the worker bees have completed their search, they tell the observation bees, who are in charge of the hive's dancing area, of the best food sources they have discovered. From the information passed on, the observer bees memorize the places where these food sources, with the largest amounts of nectar, can be found. Then, all information presented by the worker bees is processed, and a food source is selected based on the probability associated with its amount of nectar, as presented in (51).

$$p_i = \frac{F(\mathbf{z}_i)}{\displaystyle\sum_{n=1}^{BN} F(\mathbf{z}_n)} \tag{51}$$

In (51), the roulette-wheel selection method is used. Furthermore, it is possible to verify that the higher the value of $F(\mathbf{z}_i)$, the greater the probability that the ith food source is selected by the algorithm.

3.2.4 Observer Bees Phase

According with the probability value p_i, as presented in (51), a new food source $\mathbf{z}_i$ can be selected. Once the food source is selected, a modification occurs in (50). If the amount of nectar found in the new food source ($\mathbf{v}_i$) is greater than or equal to that obtained in the previous step ($\mathbf{z}_i$), it will replace $\mathbf{z}_i$ and will join the population as a new member.

3.2.5 Explorer Bees Phase

If the newly selected food source represented by $\mathbf{z}_i$ is not able to be improved after a pre-defined number of iterations,
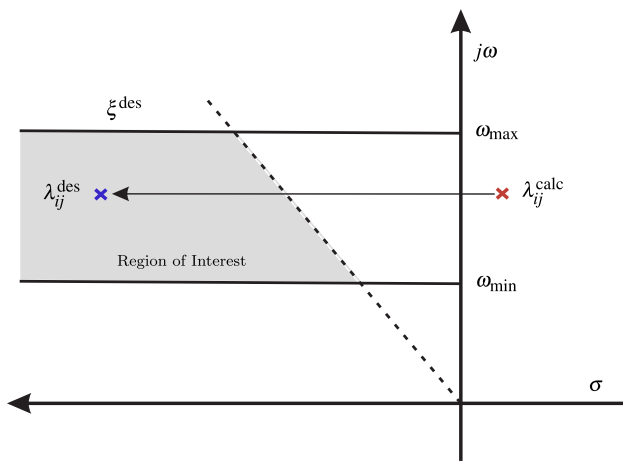
Fig. 8 Region of interest for the eigenvalues

Parameters of the POD

$$\mathbf{z}_i = \begin{array}{|c|c|c|c|c|c|c|c|c|c|c|c|c|c|} \hline T_1^u & K_1^u & T_3^u & K_3^u & T_1^{\mathrm{pod}} & T_2^{\mathrm{pod}} & K^{\mathrm{pod}} & T_{1_1}^{\mathrm{pss}} & T_{2_1}^{\mathrm{pss}} & K_1^{\mathrm{pss}} & \cdots & T_{1_{np}}^{\mathrm{pss}} & T_{2_{np}}^{\mathrm{pss}} & K_{np}^{\mathrm{pss}} \\ \hline \end{array}$$

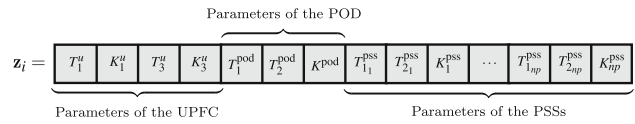Parameters of the UPFC   Parameters of the PSSs

Fig. 9 Representation of a solution proposal

as input values to evaluate the functions $F_1(\mathbf{z}_i)$ and $F_2(\mathbf{z}_i)$, defined in (52) and (53).

$$F_1(\mathbf{z}_i) = \sum_{j=1}^{p} \left| \xi^{\mathrm{des}} - \min(\xi_j) \right| \qquad (52)$$

$$F_2(\mathbf{z}_i) = \sum_{j=1}^{p} \sum_{i=1}^{n} \left| \lambda_{ij}^{\mathrm{des}} - \lambda_{ij}^{\mathrm{calc}} \right| \qquad (53)$$

For the proposed optimization problem, the function $F(\mathbf{z}_i)$, composed of $F_1(\mathbf{z}_i)$ and $F_2(\mathbf{z}_i)$, is properly defined as shown in (54), in which $\eta_1 = \eta_2 = 1$ are weighting coefficients empirically chosen.

$$\text{minimize} \quad F(\mathbf{z}_i) = \eta_1 F_1(\mathbf{z}_i) + \eta_2 F_2(\mathbf{z}_i) \qquad (54)$$

A power system with ng generators equipped with np PSSs and a UPFC–POD was considered. The optimization algorithms must provide a solution with a set of gains and time constants for each PSS controller, for the POD, and for the PI controllers of the UPFC. In this way, the obtained solution is represented by a vector, $\mathbf{z}_i$, with the parameters of ns supplementary damping controllers, as shown in Fig. 9.

4 Problem Formulation

For a power system to present a safe margin of operation for small-signal disturbances, the damping coefficients, ξ_i, of its low-frequency oscillatory modes must be sufficiently high for any operating point within its typical loading range. Therefore, the objective function $F(\mathbf{z}_i)$ should allow the optimization algorithm to conduct the search in the solution space of the problem and, consequently, determine an adjustment for the parameters of the supplementary damping controllers under different loading conditions. This ensures a minimum desired damping, ξ^{des}, for any operating point within the specified range. Also, it must ensure that the frequencies of the oscillatory modes of interest, ω^{calc}, obtained at the end of the parametrization process, do not show significant differences in comparison to those frequencies that were calculated without the use of controllers. In this sense, two objective functions, $F_1(\mathbf{z}_i)$ and $F_2(\mathbf{z}_i)$, will be defined, associated with the main objective function $F(\mathbf{z}_i)$, which will be responsible, respectively, for the minimum desired damping and for the frequencies of the oscillatory modes of interest present in the power system. Thus, for each iteration of the optimization algorithm, the eigenvalues of the simulated system must be selected and allocated within a specific region in the complex plane, as shown in Fig. 8.

From these considerations, at each iteration, two matrices will be defined, with dimensions $q \times p$ and $n \times p$. The first one will consist of the q damping coefficients of the system and the second of the n eigenvalues of interests, λ^{calc}, both at the p specified operation points. These matrices will be used

5 Test and Results

This section presents the results obtained from the simulations carried out using the algorithms presented in Sect. 3 applied to the coordinated parametrization of the supplementary damping controllers and PI controllers of the UPFC considering different operational scenarios.

The proposed models and optimization algorithms were implemented in MATLAB R2019a using a computer with a 3.20 GHz Intel® Core™ i7-8700 processor and 32 GB of RAM.

5.1 Analysis of the New England System

Static and dynamic analysis of the New England system (Fortes et al., 2016) are conducted. The single-line diagram of this system is shown in Fig. 10. The UPFC–POD set is allocated between buses 37 and 38 in one of the transmission lines that connect areas 1 and 2. This location is justified by its proximity to the region that has the worst voltage levels of the system. Also, the transmission line that connects buses
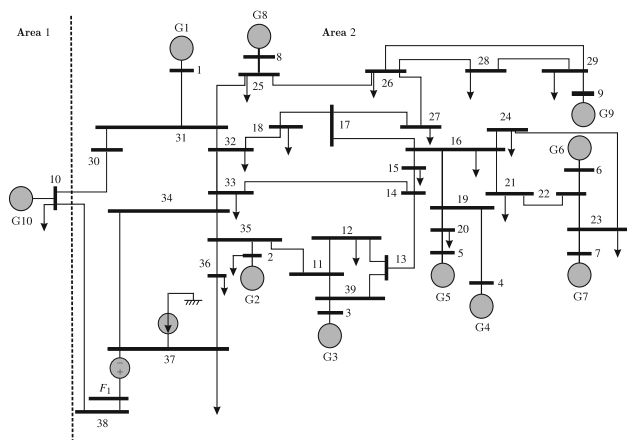
Fig. 10 Single-line diagram of the New England system

37 and 38 has a high inductive reactance compared to the other lines, which allows a greater margin of reactive compensation by the UPFC in addition to introducing additional damping to the interarea mode.

The value of the coupling reactance of the transformer connecting the VSC1 to the transmission line (positioned between buses 37 and F_1) is 0.01 p.u. The values of the parameters of the UPFC control structure (K_1^u, K_2^u, K_3^u, T_1^u, T_2^u, and T_3^u) will be determined by the optimization algorithms and T_m^{pod} is 0.001 p.u. When the UPFC is allocated in the power system but does not actuate over the voltage and the power flows (a situation that will be called the *base case*), the variables related to the VSCs present values equal to zero.

In this work, five different loading levels are defined (80%, 90%, 100%, 110%, and 120%) in relation to the specified nominal load level for this system. For this operating range, the voltage profile on the buses of the system is presented in Fig. 11.

By analyzing Fig. 11a it is possible to infer that, in the condition of higher loading (120 %), the power system has voltage magnitudes at buses 11, 12, 13, 14, 15, 33, 34, 35, 36, and 37 outside the acceptable operating limits (0.95 – 1.05 p.u.). This violation can cause voltage instability if a major disturbance occurs. In this operating condition (without power flow control) the power flow on line $F_1 - 38$ is $-19.05 - j138.64$ MVA. To solve the voltage problem, the UPFC was installed between buses 37 and F_1 and, after its actuation in the management of the power flow on line F_1-38 ($-75 - j150$ MVA) and in the voltage magnitude at bus 37 (1.0 p.u.) we have a new voltage profile for the system, shown in Fig. 11b. By analyzing Fig. 11b it can be verified that the undervoltage problem at the marked buses in the high loading condition was corrected, and the voltage profile remains within the recommended range. In this operating condition, the control variables of the UPFC assume the val-
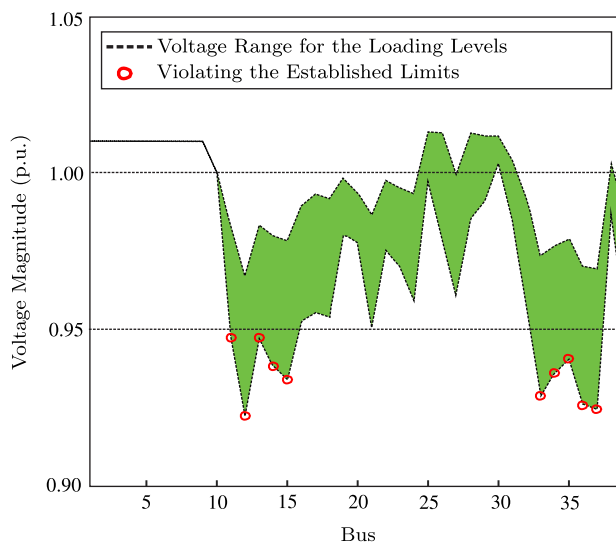
(a)
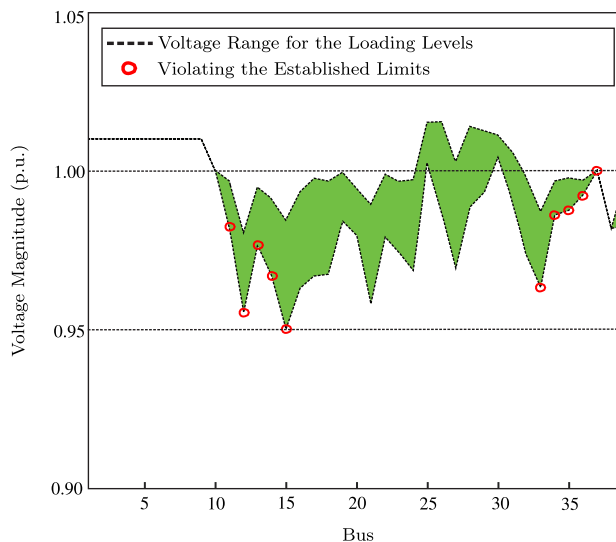
(b)

Fig. 11 Voltage profile in the New England system for the specified loading range **a** without and **b** with the actuation of the UPFC

ues of $V_p = -0.097$ p.u., $V_q = -0.094$ p.u., and $I_q = 3.775$ p.u.

For the base case operating at nominal loading, the eigenvalues of interest, obtained from the state matrix of the power system, are shown in Table 1, as well as the oscillation frequencies, ω_{ni}, and the associated damping coefficients, ξ_i.

The eigenvalues shown in Table 1 indicate that the system has, for this point of operation, nine oscillatory modes, of which eight are local ($L1$–$L8$) and one is interarea ($I1$). Moreover, three of the local modes are unstable ($L1$–$L3$) while the other ones have low damping rates (less than 4 %). This analysis allows characterizing the system with an oscil-

Table 1 Dominant eigenvalues, undamped natural frequencies, and base case damping coefficients for nominal loading

Modes	Eigenvalues	ξ_i (p.u.)	ω_{ni} (Hz)
L_1	$0.1550 \pm j5.9610$	-0.0260	0.9490
L_2	$0.1150 \pm j6.3970$	-0.0180	1.0183
L_3	$0.0749 \pm j6.9225$	-0.0108	1.1018
I_1	$-0.0068 \pm j3.5036$	0.0020	0.5576
L_4	$-0.1108 \pm j6.5207$	0.0170	1.0380
L_5	$-0.1880 \pm j8.3228$	0.0226	1.3249
L_6	$-0.2423 \pm j8.3737$	0.0289	1.3333
L_7	$-0.2116 \pm j7.2181$	0.0293	1.1493
L_8	$-0.2748 \pm j8.1546$	0.0337	1.2986

latory instability for the operating condition in the nominal loading.

To correct the oscillatory instability verified in the power system, nine PSSs are installed at generators $G1$–$G9$ and a POD controller is installed at the UPFC. The local input signal adopted for the POD is the variation of the active power that flows through the line $37 - 34$.

5.2 Evaluation of the Performances of the Methods

To define the adjustment of the supplementary controllers, five operating points will be evaluated within the established loading range (80–120%) with the UPFC actuating and considering a minimum damping of 15% ($\xi^{des} = 15\%$). For both algorithms the maximum number of iterations is equal to 1000, and the population size for both of them was 20.

For the parametrization of the FA, the following values were considered: $\beta_0 = 2.0$, $\alpha = 0.5$, and $\gamma = 1.0$.

In both algorithms, a set of constraints was imposed on the adjustment of time constants (seconds) and gains (p.u.), as shown in Table 2.

To evaluate the performance of the ABC algorithm and FA, 25 tests were performed for each of them, using the objective function defined in (54). The data presented in Table 3 was obtained from two types of analysis. The first is specific to the set of tests that produced adjustments that led the power system to the desired damping, i.e., that returned $\xi^{min} = \xi^{des} \pm 10\%$, which is equivalent to a minimum damping within the range of [14.85%, 15.15%]. The second includes all the tests and offers a general statistical overview of the results determined by each algorithm after 1000 iterations.

The analysis of the data presented in Table 3 indicates that the adjustment obtained by the FA leads the power system to operate within the specified damping range in 20 of the 25 tests performed while the ABC algorithm was successful in only 14 tests. According to Table 3, when analyzing the statistical results of the set of minimum damping produced by all the tests (after 1000 iterations), it appears that the FA performs slightly better than the ABC algorithm. The average computational times of the ABC algorithm and FA to solve the problem considering $\xi^{min} = \xi^{des} \pm 10\%$ were 0.38h and 0.17h, respectively.

Figure 12 shows the average evolutions of the minimum damping coefficient of the power system, with a confidence interval of 95%, as a function of the iteration number, determined by (a) the ABC algorithm and (b) the FA, respectively.

**Table 2** Bounds for the PI, PSSs, and POD control parameters

	Parameters	T_1^{pod}	T_2^{pod}	K^{pod}	T_1^u	T_3^u	K_1^u	K_3^u	$T_{1_k}^{pss}$	$T_{2_k}^{pss}$	K_k^{pss}
Bounds	Minimum	0.01	0.25	0.10	0.001	0.01	0.001	1.00	0.50	0.01	1.00
	Maximum	0.25	0.50	0.50	0.100	1.00	0.500	10.0	1.50	0.50	15.00

Table 3 Performance comparison of algorithms for 25 trials

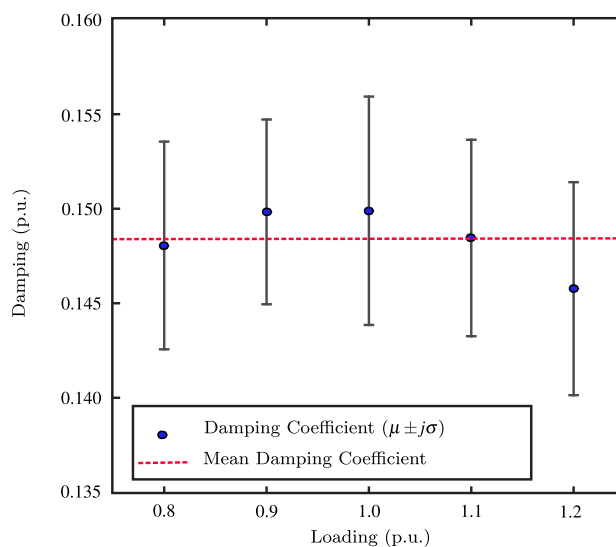| Minimum damping (ξ^{min})	Comparative performance criteria	Method		ABC	FA
$\xi^{des} \pm 10\%$	1	Number of solutions with $\xi^{min} = \xi^{des} \pm 10\%$		14	20
	2	Number of iterations	Minimum	359	21
			Mean	381	176
			Maximum	899	981
Any	3	Damping coefficient (p.u.)	Best	0.1503	0.1500
			Worst	0.1317	0.1320
			Mean	0.1457	0.1478
			Median	0.1490	0.1500
			Standard deviation	0.0056	0.0047
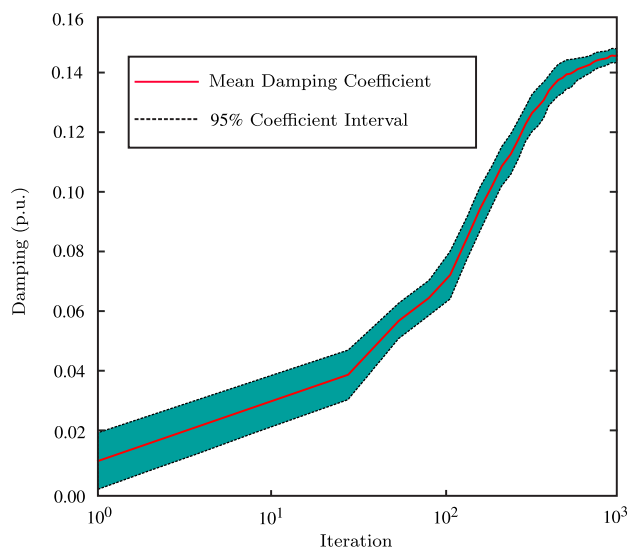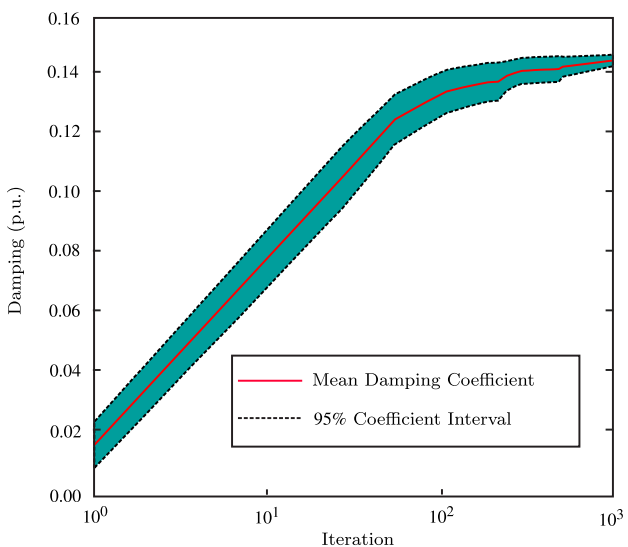
Fig. 12 Average evolution of the damping coefficients with **a** the ABC algorithm, and **b** with the FA

Fig. 13 Range of the minimum damping coefficients for different loading scenarios with **a** the ABC algorithm, and **b** with the FA
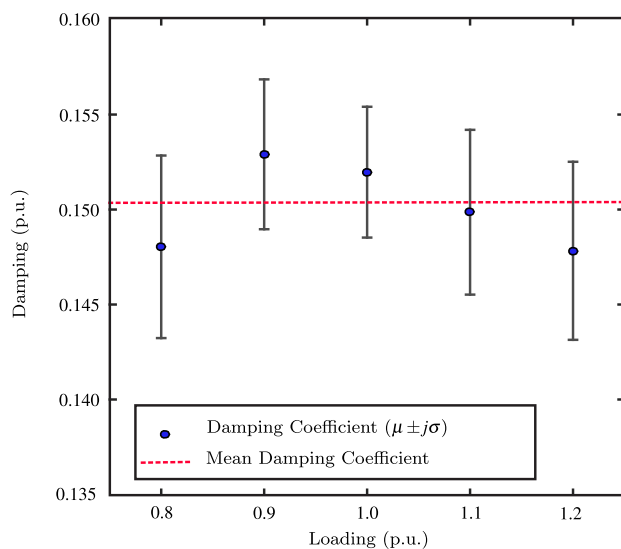
It corroborates the conclusions previously obtained about the necessity of a smaller number of iterations, on average, for the convergence of the FA.

Figure 13 shows, for each of the five loading levels evaluated, the average minimum damping and its respective error (represented by the standard deviation), considering the set of 25 tests performed (after 1000 iterations) and the overall average damping of these five levels (dashed line).

When analyzing Fig. 13, it is reasonable to conclude that the FA performed better than the ABC algorithm, since its adjustments generated better minimum damping for most of the loading levels considered. Besides, the average minimum

damping of the five loading levels analyzed (dashed line) was closer to the desired damping (ξ^{des}).

To define which of the optimization algorithms is the most efficient (under the conditions established in this work) for the task of determining suitable adjustment parameters of the PSSs, UPFC–POD, and PI controllers for the New England test system, by specifying minimum damping (considering the five loading levels), for low-frequency oscillatory modes, four criteria were used (the first two can be seen in Table 3 and the third in Fig. 13: (1) higher number of adjustments that guarantee minimum damping within the range between 14.85% and 15.15%; (2) damping coefficients closer to the

Table 4 Gains (p.u.) and time constants (s) for the PSSs parametrized with the FA

Parameters	PSS G1	PSS G2	PSS G3	PSS G4	PSS G5	PSS G6	PSS G7	PSS G8	PSS G9
$T_1^{pss} = T_3^{pss}$	1.0173	0.9374	0.7131	0.8955	0.5632	0.8197	0.8117	0.6674	0.8410
$T_2^{pss} = T_4^{pss}$	0.0337	0.1227	0.1517	0.0140	0.2587	0.0977	0.2837	0.0848	0.4081
K^{pss}	10.5685	5.3601	4.2186	8.9316	4.5757	9.8772	1.0005	4.5640	7.7345

Table 5 Gains (p.u.) and time constants (s) for the PI and POD controllers parametrized with the FA

Parameters of the UPFC–POD			Parameters of the PIs				
$T_1^{pod} = T_3^{pod}$	$T_2^{pod} = T_4^{pod}$	K^{pod}	$T_1^u = T_2^u$	T_3^u	$K_1^u = K_2^u$	K_3^u	T_m^{pod}
0.1457	0.4551	0.3787	0.0597	0.0128	0.0206	5.6975	0.0010

Table 6 Dominant eigenvalues, undamped natural frequencies, and damping coefficients for the base case under nominal loading

Modes	Eigenvalues	ξ_i (p.u.)	ω_{ni} (Hz)
L_1	$-0.9971 \pm j5.9137$	0.1663	0.9545
L_2	$-1.1030 \pm j6.3485$	0.1712	1.0255
L_3	$-1.0934 \pm j6.9435$	0.1555	1.1187
I_1	$-0.5808 \pm j3.4849$	0.1644	0.5623
L_4	$-1.2572 \pm j6.6991$	0.1845	1.0848
L_5	$-1.2987 \pm j8.2684$	0.1552	1.3321
L_6	$-1.2815 \pm j8.4328$	0.1502	1.3575
L_7	$-1.1366 \pm j7.4300$	0.1512	1.1963
L_8	$-1.6010 \pm j7.9791$	0.1967	1.2952

specified values (considering the 25 tests), i.e., with the best average and the smallest standard deviation; and (3) a global average of the minimum damping for the specified loading levels closest to ξ^{des}. The FA performed better than the ABC algorithm in all the three considered criteria. Thus, it is possible to conclude that the FA has a better performance than the ABC algorithm, being, therefore, accredited as a tool for the parametrization of the supplementary damping controllers.

5.3 Small-Signal Stability Analysis

After verifying that the FA presents better performance than the ABC algorithm, the set of parameters used for the adjustment of the controllers was obtained in the test that showed the least dispersion for the values of the minimum damping (for the five operating points established), after 1000 iterations. The adjusted parameters of the PSSs, UPFC–POD, and PI controllers provided by the FA for the chosen test scenario are shown in Tables 4 and 5.

For the nominal load level and after parametrization of the supplementary damping controllers, it is possible to observe from Table 6 that the power system, previously unstable (see Table 1), starts to operate stably within the damping range specified. The region of allocation in the complex plane of

the eigenvalues of interest for the two cases studied (Fig. 14) reinforces this conclusion.

The high margin of stability in the face of small-signal disturbances provided by the proposed solution can be observed when the mechanical power of the generator $G1$ undergoes a (step) disturbance of 0.05 p.u. In this situation, the response of the variation in the angular speed of the generator G1 against the reference generator ($G2$) can be seen in Fig. 15.

To evaluate the minimum damping of the power system (with the parametrization of the supplementary controllers according to Tables 4 and 5), in operating conditions different from those considered by the FA in the optimization process, but within the evaluated range (80–120% of loading for the base case), 17 operating points were considered, as it can be seen in Fig. 16.

By analyzing Fig. 16, it is possible to conclude that the minimum damping of the power system remains practically unchanged, and around what was specified, even when considering the load variation. On the other hand, there is a clear modification in the range when it comes to the maximum damping of the eigenvalues of interest, which is logical given that there is no control over its value.

Moreover, the obtained parametrization provides high damping in all cases, demonstrating the effectiveness and robustness of the solution obtained by the FA.

6 Conclusions

This article evaluated the performance of the artificial bee colony (ABC) algorithm and the firefly algorithm (FA) for conducting a coordinated parametrization of the proportional-integral (PI) controllers of the unified power flow controller (UPFC) and supplementary damping controllers. A current injection model for the UPFC was also presented, which can be utilized in both static and dynamic studies in power systems.
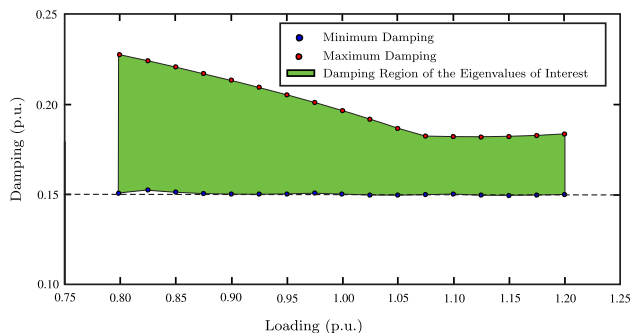
Static analysis evaluated the performance of the proposed model for the UPFC installed in the New England system.
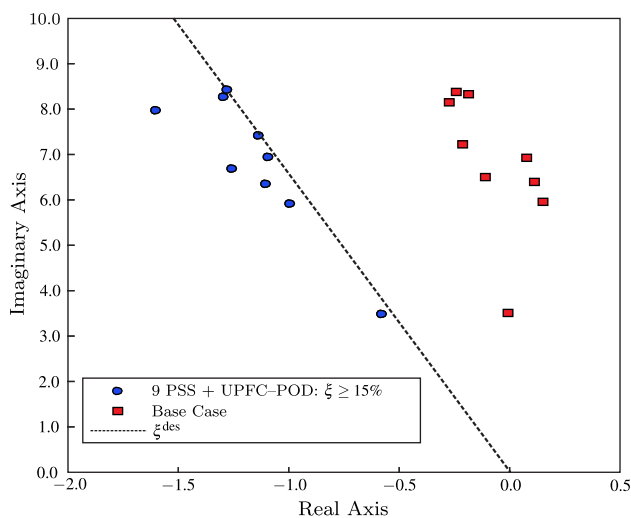
Fig. 14 Location of the eigenvalues of interest after the parametrization of the PSSs, PI, and UPFC–POD controllers
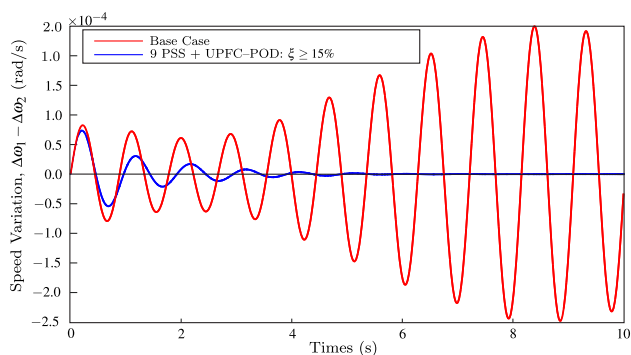
Fig. 15 Angular speed variation $\Delta\omega_1 - \Delta\omega_2$

Fig. 16 Minimum and maximum damping of the eigenvalues of interest as a function of the loading of the power system

It was possible to verify, from the simulations, significant improvements in the voltage profile and an increase in the voltage stability margin of the power system. It was also concluded that the UPFC actuated effectively in the control of both the active and reactive power flows in the respective installation buses.

Regarding the dynamic analysis performed, the two optimization algorithms had their performance compared through statistical indicators. The objective was to carry out a robust parametrization of the PI and supplementary damping controllers, considering different loading scenarios. From the obtained results, it was possible to conclude that the FA was more efficient than the ABC algorithm according to the criteria evaluated during the tests performed, showing that the system remained stable, even after loading variation, with damping greater than the specified in the project, demonstrating the robustness of the parametrization provided by the FA. Therefore, it is possible to accredit the FA as a powerful tool in the study of small-signal stability in electric power systems. Future works will include the modeling of intermittent renewable generation, such as wind and photovoltaic, in the formulation of the problem.

Declarations

References

Anderson, P., & Fouad, A. A. (2003). *Power system control and stability* (2nd ed.). Piscataway: Wiley-IEEE Press. A John Wiley & Sons.

DeMello, F. P., & Concordia, C. (1969). Concepts of synchronous machine stability as affected by excitation control. *IEEE Transactions on Power Apparatus and Systems, PAS–88*(4), 316–329. https://doi.org/10.1109/tpas.1969.292452.

Devarapalli, R., & Bhattacharyya, B. (2021). Power and energy system oscillation damping using multi-verse optimization. *SN Applied Sciences, 3*(3), 1–18. https://doi.org/10.1007/s42452-021-04349-2

Eslami, M., Shareef, H., Taha, M. R., & Khajehzadeh, M. (2014). Adaptive particle swarm optimization for simultaneous design of UPFC damping controllers. *International Journal of Electrical Power & Energy Systems, 57*, 116–128. https://doi.org/10.1016/j.ijepes.2013.11.034

Fazeli-Nejad, S., Shahgholian, G., & Moazzami, M. (2019). Artificial bee colony algorithm based approach for power system oscillation damping with PSS and STATCOM. *International Journal of Research Studies in Electrical and Electronics Engineering, 5*(2), 27–39. https://doi.org/10.20431/2454-9436.0502004

Fortes, E. V., Araujo, P. B., & Macedo, L. H. (2016). Coordinated tuning of the parameters of PI, PSS and POD controllers using a specialized Chu-Beasley's genetic algorithm. *Electric Power Sys-*

tems Research, 140, 708–721. https://doi.org/10.1016/j.epsr.2016.04.019

Fortes, E.V., Araujo, P.B., Macedo, L.H., Gamino, B.R., & Martins, L.F.B. (2016). Analysis of the influence of PSS and IPFC–POD controllers in small-signal stability using a simulated annealing algorithm. In: 2016 12th IEEE international conference on industry applications (INDUSCON), pp. 1–8. IEEE. https://doi.org/10.1109/induscon.2016.7874512.

Fortes, E. V., Macedo, L. H., Araujo, P. B., & Romero, R. (2018). A VNS algorithm for the design of supplementary damping controllers for small-signal stability analysis. *International Journal of Electrical Power & Energy Systems, 94*, 41–56. https://doi.org/10.1016/j.ijepes.2017.06.017

Gamino, B. R., & Araujo, P. B. (2017). Application of a basic variable neighborhood search algorithm in the coordinated tuning of PSS and POD controllers. *Journal of Control, Automation and Electrical Systems, 28*(4), 470–481. https://doi.org/10.1007/s40313-017-0321-3

Guesmi, T., Alshammari, B. M., Almalaq, Y., Alateeq, A., & Alqunun, K. (2021). New coordinated tuning of SVC and PSSs in multimachine power system using coyote optimization algorithm. *Sustainability, 13*(6), 3131. https://doi.org/10.3390/su13063131

Heffron, W. G., & Phillips, R. A. (1952). Effect of a modern amplidyne voltage regulator on underexcited operation of large turbine generators [includes discussion]. *Transactions of the American Institute of Electrical Engineers. Part III: Power Apparatus and Systems, 71*(3), 692–697. https://doi.org/10.1109/aieepas.1952.4498530

Hingorani, N. (2000). *Understanding FACTS?: Concepts and technology of flexible AC transmission systems*. New York: IEEE Press.

Huang, Z., Ni, Y., Shen, C. M., Wu, F. F., Chen, S., & Zhang, B. (2000). Application of unified power flow controller in interconnected power systems-modeling, interface, control strategy, and case study. *IEEE Transactions on Power Systems, 15*(2), 817–824. https://doi.org/10.1109/59.867179

Kar, M. K., Kumar, S., Singh, A. K., & Panigrahi, S. (2021). A modified sine cosine algorithm with ensemble search agent updating schemes for small signal stability analysis. *International Transactions on Electrical Energy Systems, 31*(11), 1–29. https://doi.org/10.1002/2050-7038.13058

Kopcak, I., Costa, V.F., & Silva, L.C.P. (2007). A generalized load flow method including the steady state characteristic of dynamic devices. In: 2007 IEEE Lausanne power tech, pp. 86–91 . https://doi.org/10.1109/PCT.2007.4538297.

Kundur, P. (1994). *Power system stability and control*. New York: McGraw-Hill.

Larsen, E., & Swann, D. (1981). Applying power system stabilizers-part II: Performance objectives and tuning concepts. *IEEE Transactions on Power Apparatus and Systems, PAS–100*(6), 3025–3033. https://doi.org/10.1109/tpas.1981.316410.

Martins, L. F. B., Araujo, P. B., Fortes, E. V., & Macedo, L. H. (2017). Design of the PI-UPFC-POD and PSS damping controllers using an artificial bee colony algorithm. *Journal of Control, Automation and Electrical Systems, 28*(6), 762–773. https://doi.org/10.1007/s40313-017-0341-z

Menezes, M. M., de Araujo, P. B., & do Valle, D. B. (2016). Design of PSS and TCSC damping controller using particle swarm optimization. *Journal of Control, Automation and Electrical Systems, 27*(5), 554–561. https://doi.org/10.1007/s40313-016-0257-z

Miotto, E.L., Araujo, P.B., Fortes, E.V., Gamino, B.R., & Martins, L.F.B. (2018). Coordinated tuning of the parameters of PSS and POD controllers using bio-inspired algorithms. IEEE Transactions on Industry Applications pp. 3845–3857. https://doi.org/10.1109/TIA.2018.2824249.

Movahedi, A., Niasar, A. H., & Gharehpetian, G. (2019). Designing SSSC, TCSC, and STATCOM controllers using AVURPSO, GSA, and GA for transient stability improvement of a multi-machine power system with PV and wind farms. *International Journal of Electrical Power & Energy Systems, 106*, 455–466. https://doi.org/10.1016/j.ijepes.2018.10.019

Naderipour, A., Abdul-Malek, Z., Ramachandaramurthy, V. K., Miveh, M. R., Moghaddam, M. J. H., & Guerrero, J. M. (2020). Optimal SSSC-based power damping inter-area oscillations using firefly and harmony search algorithms. *Scientific Reports, 10*(1), 1–11. https://doi.org/10.1038/s41598-020-69123-7

Noroozian, M., Angquist, L., Ghandhari, M., & Andersson, G. (1997). Use of UPFC for optimal power flow control. *IEEE Transactions on Power Delivery, 12*(4), 1629–1634. https://doi.org/10.1109/61.634183

Rahman, M.M., Ahmed, A., Galib, M.M.H., & Moniruzzaman, M. (2021). Optimal damping for generalized unified power flow controller equipped single machine infinite bus system for addressing low frequency oscillation. ISA Transactions pp. 97–112 . https://doi.org/10.1016/j.isatra.2021.01.031.

Sabo, A., Wahab, N. I. A., Othman, M. L., Jaffar, M. Z. A. M., & Beiranvand, H. (2020). Optimal design of power system stabilizer for multimachine power system using farmland fertility algorithm. *International Transactions on Electrical Energy Systems, 30*(12), 1–33. https://doi.org/10.1002/2050-7038.12657

Singh, M., Patel, R., & Neema, D. (2019). Robust tuning of excitation controller for stability enhancement using multi-objective meta-heuristic firefly algorithm. *Swarm and Evolutionary Computation, 44*, 136–147. https://doi.org/10.1016/j.swevo.2018.01.010

Takahashi, A.L.M., Fortes, E.V., Araujo, P.B., Miotto, E.L., & Martins, L.F.B. (2018). A current sensitivity model for power system stability studies. In: 2018 13th IEEE international conference on industry applications (INDUSCON), pp. 955–962. IEEE . https://doi.org/10.1109/induscon.2018.8627348.

Valle, D., & Araujo, P. (2015). The influence of GUPFC FACTS device on small signal stability of the electrical power systems. *International Journal of Electrical Power & Energy Systems, 65*, 299–306. https://doi.org/10.1016/j.ijepes.2014.10.012

Verdejo, H., Pino, V., Kliemann, W., Becker, C., & Delpiano, J. (2020). Implementation of particle swarm optimization (PSO) algorithm for tuning of power system stabilizers in multimachine electric power systems. *Energies, 13*(8), 2093. https://doi.org/10.3390/en13082093

Watanabe, O. (2009). *Stochastic algorithms: foundations and applications*. Berlin: Springer.

Yang, N., Liu, Q., & McClley, J. D. (1998). TCSC controller design for damping interarea oscillations. *IEEE Transactions on Power System, 13*(14), 1304–1310. https://doi.org/10.1109/59.736269

Yang, X.S. (2008). Nature-inspired metaheuristic algorithms. Luniver Press.

Zhenenko, G., & Farah, H. (1984). Simultaneous optimization of the adjustable parameters in multimachine power systems. *Electric Power Systems Research, 7*(2), 103–108. https://doi.org/10.1016/0378-7796(84)90019-1